Numerical Study on Influences of Barrier Arrangements on Dielectric Barrier Discharge Characteristics

Woo Seok Kang, Jin Myung Park, Yongho Kim, and Sang Hee Hong, *Member, IEEE*

***Abstract*—A numerical study has been carried out to understand the influences of barrier arrangements on the discharge characteristics of dielectric barrier discharge (DBD). A 1.5-dimensional (1.5-D) modeling is considered in the arrangements of bare, single-barrier, and double-barrier electrodes while a two-dimensional (2-D) approach is employed in a configuration of ferroelectric packed discharge (FPD). Numerical simulations show that the evolution of microdischarges in DBD occurs sequentially in the three distinctive phases of avalanche, streamer, and decay, and that the dielectric barriers make streamer discharges stabilized and sustained in lowered electric fields without transition to spark compared with no barrier case. Especially, the highly nonuniform strong electric field effect created by the pellets appears to be formed in FPD, which enables the flue gas cleaning to be expected to enhance the decomposition efficiency.**

***Index Terms*—Barrier arrangement effect, dielectric barrier discharge (DBD), ferroelectric packed discharge (FPD), numerical modeling.**

I. Introduction

THE DIELECTRIC barrier discharge (DBD) is one of the important sources for generating nonequilibrium plasmas in the atmospheric pressure [1]. As a typical example of its practical application to the daily life, it has been successfully used to commercialize the production of ozone for air cleaning and sterilization during the past century. Recently, with the renewed interests in applications of atmospheric nonequilibrium plasmas [2], [3], a great deal of effort has been attempted to use the DBD in other applications such as flue gas decomposition, surface treatments, high-power lasers, eximer UV light sources, and plasma display panels [4].

Several technical methods have been suggested to control electron energy for generating the effective nonequilibrium atmospheric-pressure plasma by the DBD usable for practical applications. One of them is a proper choice of barrier materials and geometry inserted between the electrodes in DBD reactors. The ferrolectric packed discharge (FPD) is another form of DBD with a pellet-geometry by inserting ferroelectric pellets between the plate-electrodes covered with dielectric barriers. Currently, the FPD is widely studied, because it is not only simpler and more economical in varying the power supply than the conventional DBD, but also highly efficient in decomposition of volatile organic compounds (VOCs) [5].

In order to understand the influences of these technical modifications on the microdischarges usually observed during DBD, numerical simulation is essential for resolving the difficulties met in the measurements due to limited range and rapid development of the discharge in DBD. To date, there have been lots of reports on numerical studies dealing with DBD. Braun *et al.* [6] explained discharge characteristics in the single barrier discharge by a 1.5-dimensional (1.5-D) approach, and Oda *et al.* [7] also analyzed a Xe excimer lamp having an arrangement of double barrier discharge by a 1.5-D way. Eliasson *et al.* [8] showed the formation and decay of single microdischarge combined with reaction chemistry in a single barrier reactor. However, it is almost rare to find direct comparisons of plasma modeling among various barrier arrangements in the parallel-plate geometry in the previous work. Even though many experimental results revealed higher decomposition rates of flue gases in FPD reactors, it is still hard to explain the ferroelectric pellet effects on the decomposition due to the geometrical complexity of reactors.

In this work, numerical modeling on the parallel-plate DBD reactors with various barrier arrangements, as shown in Fig. 1, is carried out to understand the influences of different barrier arrangements on the evolution and characteristics of discharges. By a 1.5-D finite-difference method (FDM), discharge characteristics are described and compared in terms of discharge currents in different discharge cases of bare electrode, single-dielectric barrier, and double dielectric barriers. On the other hand, a two-dimensional (2-D) finite-element method (FEM) is used for the FPD modeling to reflect its complex pellet geometry, and the ferroelectric pellet effects are discussed with electron density and electric field in the single and double pellet cases.

Manuscript received November 7, 2002; revised April 18, 2003.

W. S. Kang is with the Department of Nuclear Engineering, Seoul National University, Seoul 151-742, Korea, and also with the Korea Institute of Science and Technology Evaluation and Planning, Seoul 137-130, Korea.

J. M. Park and S. H. Hong are with the Department of Nuclear Engineering, Seoul National University, Seoul 151-742, Korea (e-mail: hongsh@snu.ac.kr).

Y. Kim is with the Department of Nuclear Engineering, Seoul National University, Seoul 151-742, Korea, and also with the Korea Institute of Machinery and Materials, Daejeon 305-343, Korea.

Digital Object Identifier 10.1109/TPS.2003.815469

II. Modeling of DBDs

A. Computational Domains

The computational domains employed in this numerical study are presented in Fig. 2. Fig. 2(a) depicts a schematic of 1.5-D single-streamer model for a parallel-plate DBD using the so-called disk method, and Fig. 2(b) describes an unstructured

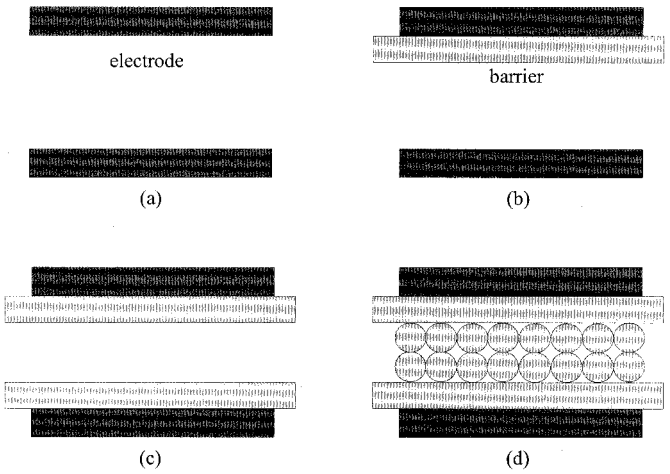

Fig. 1. Parallel-plate DBD reactors with various barrier arrangements. (a) Bare electrodes. (b) Single dielectric barrier. (c) Double dielectric barriers. (d) Ferroelectric pellets packed in the discharge gap.

triangular grid system in a 2-D model for FPD with double pellets inside a double-barrier DBD reactor. In the 1.5-D model, the dielectric barriers with relative permittivity ε_r are placed on the anode and cathode surfaces which are located at $x = 0$ and $x = d$, respectively, and the locations of barrier surfaces exposed to air in the discharge gap $(b_1 < x < b_2)$ are assumed to be b_1 and b_2. Voltage drops across the barriers are represented as V_{b1} and V_{b2}, and V_d is the discharge voltages between the barriers. In the 2-D model, the two electrodes at the top and bottom of the chamber are covered with dielectric materials, and a single pellet or double ones placed on the cathode dielectric barrier surface.

B. Fluid Equations

The motions of electrons, positive ions, and negative ions in DBD are described by a set of the following continuity equations [9], [10]:

$$\frac{\partial n_e}{\partial t} = -\nabla \cdot (n_e \mathbf{v_e}) + \nabla \cdot (D_e \nabla n_e) + (1+\gamma)\alpha n_e |\mathbf{v_e}| - \eta n_e |\mathbf{v_e}| \quad (1)$$

$$\frac{\partial n_p}{\partial t} = -\nabla \cdot (n_p \mathbf{v_p}) + (1+\gamma)\alpha n_e |\mathbf{v_e}| \quad (2)$$

$$\frac{\partial n_n}{\partial t} = -\nabla \cdot (n_n \mathbf{v_n}) + \eta n_e |\mathbf{v_e}| \quad (3)$$

where n_e, n_p, and n_n are the number densities of electron, positive ion, and negative ion, respectively. $\mathbf{v_e}, \mathbf{v_p}$, and $\mathbf{v_n}$ are the drift velocities of plasma species, and D_e is the diffusion coefficient of electron. α and η are the coefficients of electron impact ionization and electron attachment, respectively, and γ is the coefficient of secondary emission.

The governing equations (1)–(3) used for the present DBD and FPD simulations only include the direct interactions of electrons and photons with neutral gas particles, such as electron impact ionization, electron attachment, and photon impact ionization. Excited molecules and their respective indirect processes, such as stepwise ionization by metastable molecules and photoexcitation, are not taken into account because the densities of such excited molecules produced by streamers still remain far below the neutral gas density in atmospheric pressure.

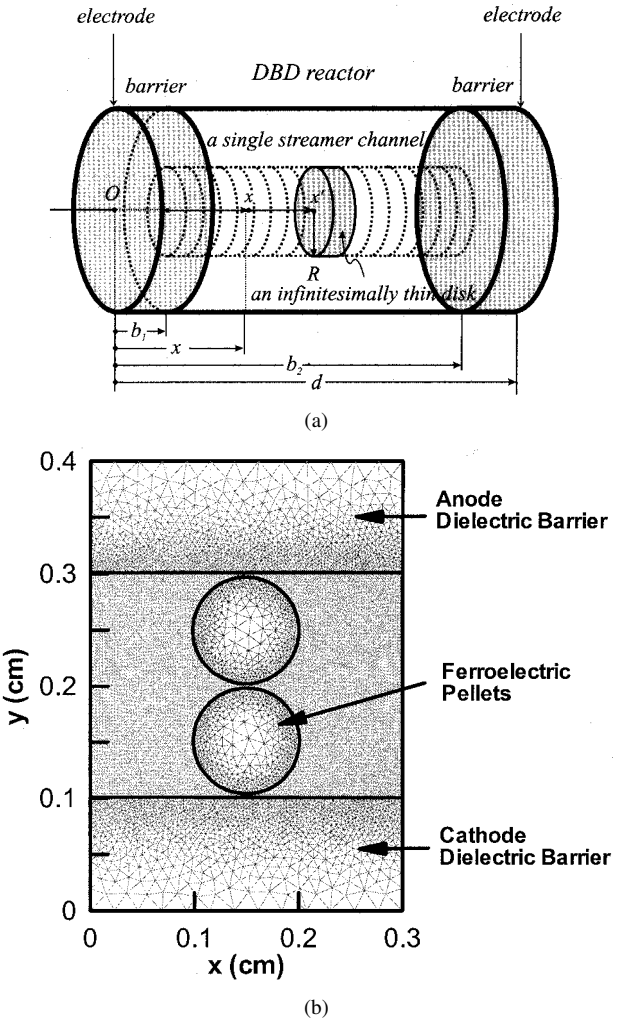

Fig. 2. (a) Schematic diagram of 1.5-D single-streamer model for DBD using the disk method. (b) Computational domain of 2-D model for FPD in an unstructured triangular grid with double pellets inside a double-barrier DBD reactor.

For simulating the discharge in an atmospheric dry air, the expressions for the transport and interaction properties appeared in (1)–(3) are presented as a function of electric field strength E in Table I [9]. Especially, the coefficient γ of secondary emission for air is chosen from the experimental results in [11].

C. Electric Field Calculations

In the 1.5-D simulation for a simple parallel-plate geometry of DBD, the disk method developed by Davies *et al.* [12] is applied since the one-dimensional (1-D) Poisson's equation has limitations to describe a discharge range during the highly localized microdischarges. The externally applied electric field E_{ext} is first obtained from Laplace's equation. Then, the electric field E_{sc} affected by space charges in the discharge range is calculated by assuming a single cylindrical channel of microdischarge as a set of infinitesimally thin disks in a streamer with radius R as depicted in Fig. 2(a)

$$E_{\text{sc}}(x) = \int_{-(x-b_1)}^{b_2} -\frac{\rho(x+x')}{2\varepsilon_0}\left(\frac{x'}{\sqrt{R^2+x^2}} \mp 1\right) dx' \quad (4)$$

TABLE I
CALCULATION DATA USED IN THIS SIMULATION FOR THE PLASMA TRANSPORT AND INTERACTION PROPERTIES [9] IN (1)–(3)

Property	Expression for Data Value
$\mathbf{v}_e$	$-6.06\times10^3 E^{0.75}$
$\mathbf{v}_p$	$2.43E$
$\mathbf{v}_n$	$-2.70E$
D_e	1800
α	$3.5\times10^3 \exp(-1.65\times10^5 E^{-1})$
η	$1.5\times10\exp(-2.50\times10^4 E^{-1})$
γ	$\psi_0 \exp(-\mu r)\theta\, pd = \psi\theta\, pd$

where σ is the surface charge density on the thin disk. The radius of streamer is assumed as 200 μm. Total electric field $E_{\rm tot}$ is then determined by the summation of $E_{\rm ext}$ and $E_{\rm sc}$.

In the 2-D simulation for FPD reflecting its geometrical complexity, the electrostatic potential ϕ and electric field $\mathbf{E}$ are calculated from Poisson's equation

$$\nabla\cdot(\varepsilon_r\nabla\phi) = -e(n_p - n_e - n_n) = -\rho \tag{5}$$

$$\mathbf{E} = -\nabla\phi \tag{6}$$

where ε_r is the relative permittivity of dielectric material, e is the charge of electron, and ρ is the net space charge in the channel.

In the 1.5-D simulation, a current equation given by Sato [13] is employed for the calculation of the current I flowing through the external circuit of the discharge reactor due to the motions of electrons and positive ions in a very short time scale of the discharge

$$I = \frac{\pi R^2 e}{d}\int (n_p|\mathbf{v_p}| + n_e|\mathbf{v_e}|)\,dx. \tag{7}$$

D. Boundary Conditions

At the plasma-barrier interfaces, all the incoming electron and ion fluxes, Γ_e and $\Gamma_{\rm ion}$, toward the dielectric barriers are assumed to be accumulated as surface charges on the barrier surfaces. Therefore, surface charge densities σ_e and $\sigma_{\rm ion}$ can be calculated from

$$\frac{\partial\sigma_e}{\partial t} = \Gamma_e\cdot\mathbf{n}, \quad \frac{\partial\sigma_{\rm ion}}{\partial t} = \Gamma_{\rm ion}\cdot\mathbf{n} \tag{8}$$

where $\mathbf{n}$ is the normal vector directed from plasma to dielectric barrier.

The boundary values of electric potential at the two electrodes are

$$\phi = V \text{ at the anode}, \quad \phi = 0 \text{ at the cathode}. \tag{9}$$

In addition, the boundary conditions of electric field and electric potential at the plasma-barrier interfaces and pellets are calculated reflecting the modifications by accumulated surface charges from Gauss' theorem with charge sources included

$$\mathbf{n}\cdot\nabla\phi - \varepsilon_r\mathbf{n}\cdot\nabla\phi_D = \frac{e}{\varepsilon_0}(\sigma_{\rm ion} - \sigma_e) \tag{10}$$

$$\mathbf{n}\times(\nabla\phi - \nabla\phi_D) = 0. \tag{11}$$

When the DBD reactor is operated in a reactor with a single barrier placed on the anode surface, the secondary emission due to photon impacts at the cathode is taken into account. In general, as is often the case with the secondary emission by ion bombardments on the cathode, the secondary emission coefficient by photon impacts $\gamma_{\rm ph}$ can be implicitly described by a current equation

$$\frac{i}{i_0} = \frac{n_e}{n_{e0}} = \frac{\exp(\alpha d)}{1 - \gamma_{\rm ph}[\exp(\alpha d) - 1]} \tag{12}$$

where

$$\gamma_{\rm ph} = \frac{\Delta g\theta}{\alpha - \mu}. \tag{13}$$

Here, Δ is the probability of effective photoelectric emission due to radiation from the gas, g is the geometrical factor which specifies the fraction of photons heading for the cathode, θ is the number of excited states owing to electron collisions per unit length in the field direction, α is the ionization coefficient, and μ is the coefficient of radiation absorption (attenuation). In numerical calculations, the electron density at the cathode is usually determined by [14]

$$n_e(d) = n_{e0} + \gamma_{\rm ph}\int \alpha n_e(x)\,dx \tag{14}$$

where n_{e0} is the peak electron density at the electrode. Although $\gamma_{\rm ph}$ is normally dependent on the electrode material and its surface condition as well as the discharge gas [15], it is assumed to be 0.01 in this numerical modeling for the bare copper electrode in atmospheric dry air. An initial value of electron density n_{e0} is taken as 10^3 cm^{-3} from an assumption that seed electrons are located just in front of the electrode at the beginning of discharge.

E. Numerical Methods

An FDM is adopted for the 1.5-D simulation of DBD by using the disk method, while an FEM is used for the 2-D simulation of FPD in the unstructured triangular grid systems for the two cases of a single ferroelectric pellet and vertically-stacked double ferroelectric pellets. A flux-corrected transport algorithm is applied, in which upwind and Lax–Wendroff schemes are used for calculations of the low- and high-order parts, respectively. Then, their numerical outcomes are corrected as the final simulation results using the method suggested by Zalesak [16].

III. NUMERICAL RESULTS AND DISCUSSION

A. Discharge Characteristics in DBD

For the 1.5-D calculations of DBD with a single barrier placed on the anode in Fig. 1(b), the thickness of a dielectric barrier with relative permittivity of 8 is 2 mm and a discharge gap is

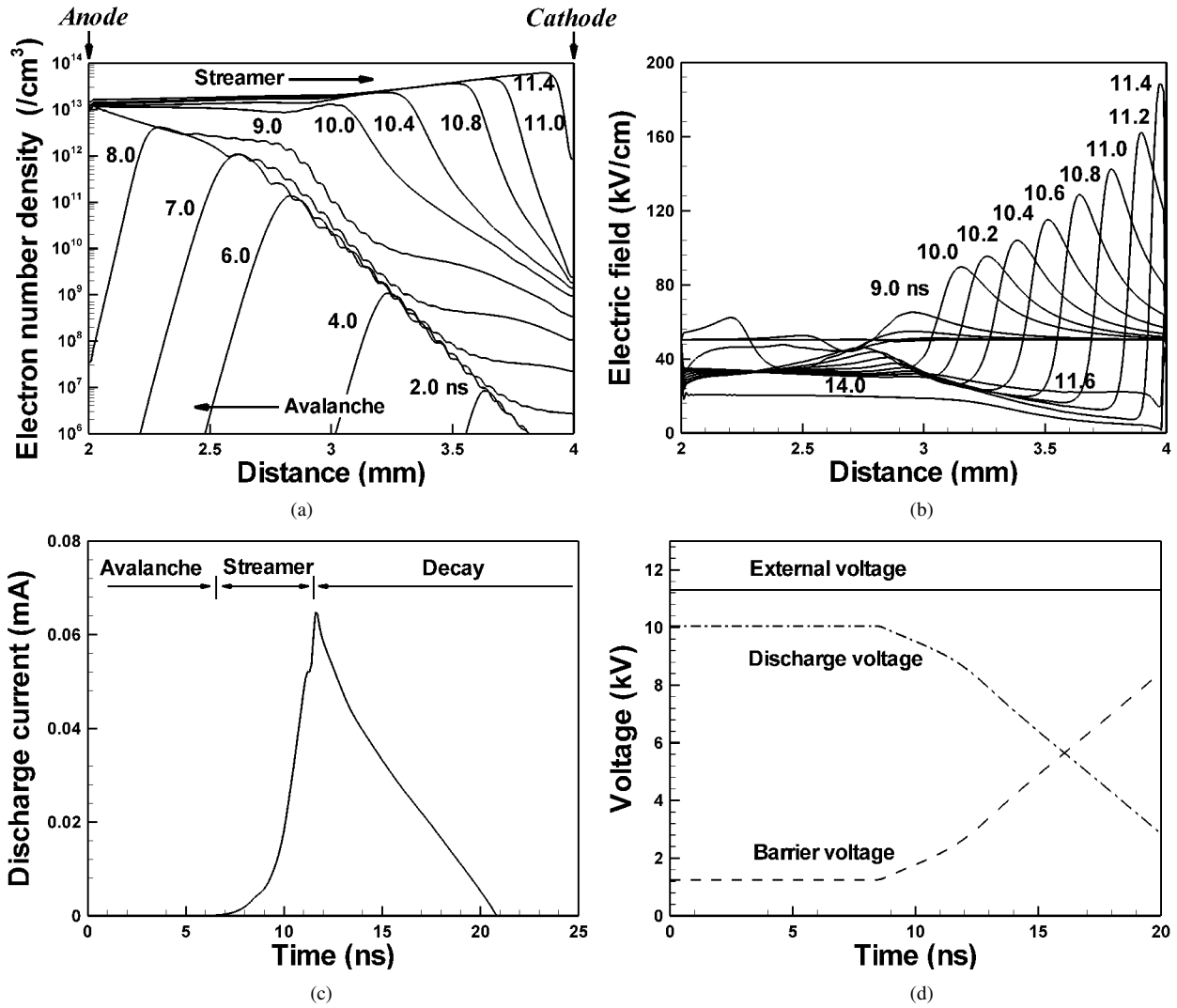

Fig. 3. Discharge characteristics in a single-barrier DBD. Temporal developments of: (a) electron number density; (b) total electric field in the streamer discharge; (c) time histories of discharge current; and (d) discharge voltages dividend by the discharge gap and barrier.

2 mm. The seed electrons are assumed to be initially distributed in front of the cathode with a Gaussian shape, of which peak electron density is 10^3 cm^{-3}. An external voltage of 11.2 kV is applied between the two electrodes to produce a uniform electric field of 50 kV/cm in the air gap in the absence of discharge.

Fig. 3 shows the evolutions of (a) electron density, (b) electric field, (c) discharge current, and (d) discharge voltage during a discharge period, respectively. The discharge characteristics in the single-barrier DBD can be classified into three phases—*avalanche, steamer*, and *decay*.

1) Avalanche Phase (0–8 ns): The seed electrons released from the cathode at $t = 0$ ns begin to drift and multiply themselves until they reach the barrier attached to the anode. Due to negligible space charge effects, there is negligible disturbance to the initial uniform electric field. Consequently, the discharge current is nearly zero and the discharge voltage sustains its initial value.

2) Streamer Phase (8–11.4 ns): After the electrons reach the barrier, a streamer formation occurs. Increase in electric field of the streamer head is observed and the discharge current begins to increase while the discharge voltage decreases. As the streamer approaches the cathode, the electric field rapidly increases and has its highest value when the streamer strikes the cathode at 11.4 ns. At this moment, the discharge current shows its maximum value, and the discharge voltage falls down while most of the external voltage appears to be applied in the barrier. Finally, a streamer channel is created between the barrier and cathode, and the electron density within the channel is about 10^{13}–10^{14} cm^{-3}.

3) Decay Phase (11.4 ns-): After the streamer phase, the electric field within the discharge region decreases and the discharge is gradually extinguished. The discharge current also decreases and finally becomes zero. This phase indicates that the accumulated surface charges on the dielectric barrier play an important role of reducing the discharge voltage.

B. Influences of Barrier Plate Arrangements on Discharge Characteristics in DBDs

Additional calculations are accomplished in the cases of bare-electrode discharge [Fig. 1(a)] and double-barrier DBD [Fig. 1(c)] to compare with single-barrier DBD [Fig. 1(b)]. The discharge gap and initial uniform electric field in each case are

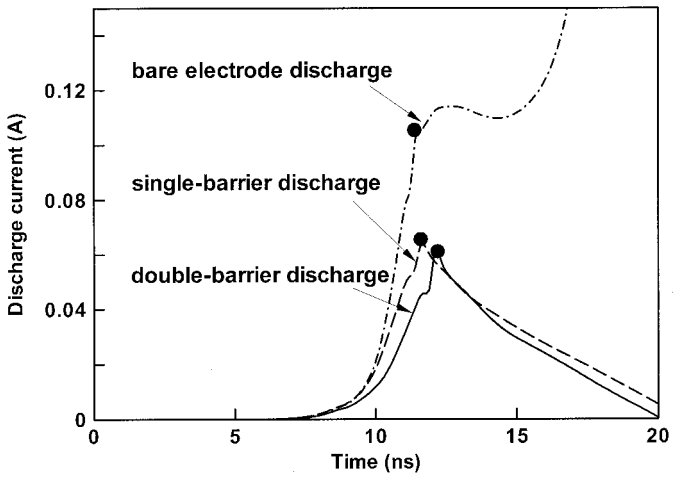

Fig. 4. Time history of discharge currents during a single-streamer discharge period in bare-electrode, single-barrier, and double-barrier discharges.

kept with the same conditions as the single-barrier case given in the previous Section III-A-1.

In the discharge current profiles, the tendencies of electron avalanche and streamer propagation are turned out to be qualitatively similar to each other in the avalanche, and streamer phase, but the different characteristics are found in the later phase. Fig. 4 shows the temporal profiles of discharge current obtained from the three cases. Discharge currents of all cases are negligibly increased up to 8 ns, among which the bare electrode discharge shows the highest value. After that, each current rapidly increases until the streamer hits a surface of the cathode or the barrier covered on the cathode and the closed circles in Fig. 4 indicate those moments. Even in this event, the bare electrode discharge still has the highest current value and finally blows up to infinity. Since the discharge voltage in the bare electrode discharge is always constant, the external electric field is also sustained. This makes overall electron density increase to a certain extent and finally the discharge comes to meet an unavoidable spark stage. On the other hand, in the barrier discharge, the discharge current decreases after its maximum point. It is, therefore, believed that the discharge voltage is lowered due to the accumulated surface charges preventing excessive discharge currents from transiting to spark.

In the double-barrier discharge, even though the effects of electrodes are removed, the current profile resembles that of the single-barrier discharge with a slightly lower current level. That is why the external electric field is reduced additionally by the accumulated surface charges on the barrier at the cathode.

C. Discharge Characteristics in FPDs

1) FPD With a Single Ferroelectric Pellet: In the present discharge case with a single pellet in the parallel-plate DBD, the diameter of ferroelectric pellet with relative permittivity of 10 is 1 mm, and the thickness of dielectric barriers with relative permittivity of 8 is 1 mm in the discharge gap distance of 2 mm. The external electric voltage applied to the electrodes is 12 kV, and a spatially uniform electron distribution of 1 cm^{-3} is used as an initial condition. Fig. 5 presents the calculated distributions of

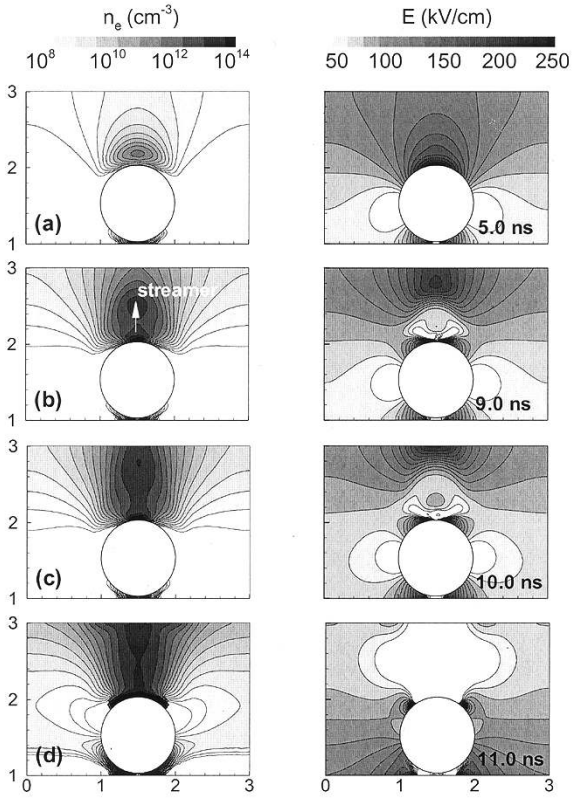

Fig. 5. Distributions of electron density (left column) and electric field strength (right column) in FPD with a single pellet inside a double-barrier DBD reactor.

electron density and electric field strength. From the beginning of discharge, the locally concentrated high electric field (about 250 kV/cm) due to the polarization of the ferroelectric pellet yields spatially nonuniform electron multiplications as seen in corona discharges, especially near the interface between pellet and cathode dielectric barrier and on the top surface of the pellet. By these multiplied electrons in the discharge region, the negative streamer start to develop like corona discharge as seen in Fig. 5(a). At 10.0 ns, the negative streamer arrives at the anode dielectric surface and a discharge channel is then created. After the streamers hit upon the dielectric and pellet surfaces, electric fields decrease in the streamer channel and the streamers propagate along the dielectric and pellet surfaces due to the highly localized electric fields on the surfaces as shown in Fig. 5(d).

2) FPD With Stacked Double Ferroelectric Pellets: When double ferroelectric pellets are used inside the double-barrier DBD reactor, they are vertically stacked between the anode and cathode dielectric barriers with the same conditions given previously. Fig. 6 shows the calculated results of the distributions of electron density and electric field strength. Similar to the single pellet case, locally concentrated nonuniform electric fields are initially created at the interfaces between the two pellets or between the pellet and plate barriers, with very high field strength up to about 350 kV/cm. After 0.9 ns, multiplied electrons at the interfaces spread themselves along the pellet surfaces. At 1.0 ns, the surface discharges appeared along the outer boundaries of barriers and pellets make electric fields decrease remaining the high-electron density.

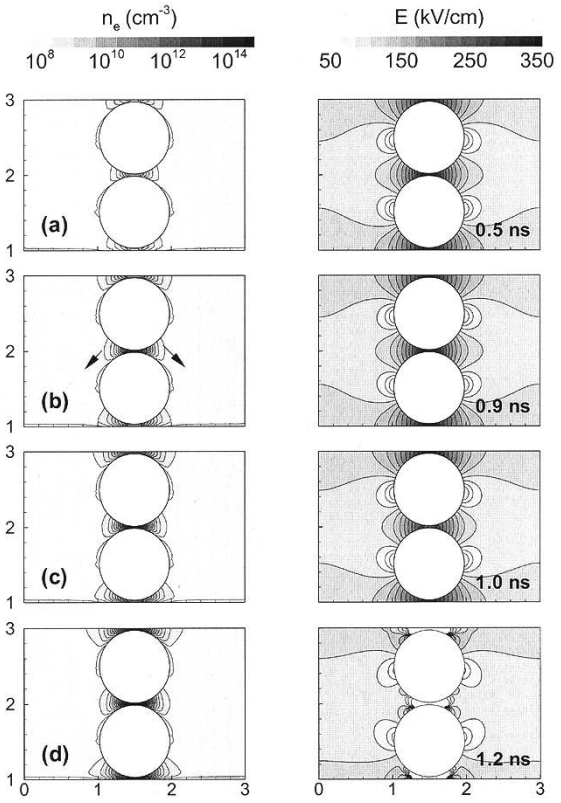

Fig. 6. Distributions of electron density (left column) and electric field strength (right column) in FPD with stacked double pellets inside a double-barrier DBD reactor.

IV. Conclusion

A numerical simulation of dielectric barrier discharges has been accomplished with surface charge behaviors on the dielectric barriers in order to understand the characteristics of microdischarges influenced by various barrier arrangements.

The geometrical effects of dielectric barriers on microdischarges have been considered by the 1.5-D FDM for DBD with parallel-plate barrier configurations, and the 2-D FEM for FPD with ferroelectric pellets. According to the simulation results, for the parallel-plate geometry with a single-barrier, the three microdischarge phases—avalanche, streamer, and decay—are observed during the discharge period. The electric field strength is enhanced as the streamer approaches the cathode, and finally, a channel is created across the discharge region in which the electron density is about 10^{13}–10^{14} cm^{-3}.

The different microdischarge characteristics have been compared in the arrangements of bare, single-barrier, and double-barrier electrodes of the DBD reactors. In the bare-electrodes case, the streamer is eventually transformed to spark with a rapid increase of discharge current. A dielectric barrier inserted between the two electrodes makes the overall electric field lower, and suppresses the transition of streamer to spark. When double-barriers are used, the electric field is lowered a bit more than that of the single-barrier case.

In the single pellet geometry of FPD, the 2-D simulation illustrates the similar effects of ferroelectric pellet as those of the plate dielectric barriers. Moreover, the pellet generates the nonuniform electric field distribution inside the discharge region and governs the discharge characteristics available in the corona discharge. In the case of FPD with stacked double pellets, only the surface discharge with high-electric field is observed. Hence, such calculated results may be a key to explain why the FPD has shown high efficiencies in flue gas decompositions resulted from the higher electron energy in the FPD due to the nonuniform electric field effect created by pellets.

References

[1] B. Eliasson and U. Kogelschatz, "Nonequilibrium volume plasma chemical processing," *IEEE Trans. Plasma Sci.*, vol. 19, pp. 1063–1077, Dec. 1991.

[2] E. E. Kunhardt, "Generation of large-volume, atmospheric-pressure nonequilibrium plasmas," *IEEE Trans. Plasma Sci.*, vol. 29, pp. 189–200, Feb. 2000.

[3] A. Schültze, J. Y. Jeong, S. E. Babayan, J. Park, G. Selwyn, and R. F. Hicks, "The atmospheric-pressure plasma jet: A review and comparison to other plasma sources," *IEEE Trans. Plasma Sci.*, vol. 26, pp. 1658–1694, Dec. 1998.

[4] U. Kogelschatz, B. Eliasson, and W. Egli, "From ozone generation to flat television screens: History and future potential of dielectric-barrier discharges," *Pure Appl. Chem.*, vol. 71, pp. 1819–1828, 1999.

[5] T. Yamamoto, P. A. Lawless, M. K. Owen, D. S. Ensor, and C. Boss, "Decomposition of volatile organic compounds by a packed-bed reactor and a pulsed corona plasma reactor," in *Non-Thermal Plasma Techniques for Pollution Control*, B. M. Penetrante and S. E. Schülthesis, Eds. Berlin, Germany: Springer-Verlag, 1993, pp. 223–238.

[6] D. Braun, U. Küchler, and G. Pietsch, "Microdischarges in air-fed ozonizers," *J. Phys. D, Appl. Phys.*, vol. 24, pp. 564–572, 1991.

[7] A. Oda, H. Sugawara, Y. Sakai, and H. Akashi, "Estimation of the light output power and efficiency of Xe barrier discharge excimer lamps using a one-dimensional fluid model for various voltage waveforms," *J. Phys. D, Appl. Phys.*, vol. 33, pp. 1507–1513, 2000.

[8] B. Eliasson and U. Kogelschatz, "Modeling and applications of silent discharge plasmas," *IEEE Trans. Plasma Sci.*, vol. 19, pp. 309–323, Dec. 1991.

[9] A. A. Kulikovsky, "Positive streamer between parallel plate electrodes in atmospheric pressure air," *J. Phys. D, Appl. Phys.*, vol. 30, pp. 441–450, 1997.

[10] P. A. Vitello, B. M. Penetrante, and J. N. Bardsley, "Simulation of negative streamer dynamics in nitrogen," *Phys. Rev. E, Stat. Phys. Plasmas Fluids Relat. Interdiscip. Top.*, vol. 49, pp. 5574–5598, 1994.

[11] G. W. Penny and G. T. Hummert, "Photoionization measurement in air, oxygen, and nitrogen," *J. Appl. Phys.*, vol. 41, pp. 572–577, 1970.

[12] A. J. Davies, C. J. Evans, and P. M. Woodison, "Computation of ionization growth at high current densities," *Proc. Inst. Elect. Eng.*, vol. 122, pp. 765–768, 1975.

[13] N. Sato, "Discharge current induced by the motion of charged particles," *J. Phys. D, Appl. Phys.*, vol. 13, pp. L3–L6, 1980.

[14] P. H. F. Morshuis, *Partial Discharge Mechanisms: Mechanisms Leading to Breakdown, Analyzed by Fast Electrical and Optical Measurements*. Delft, The Netherlands: Delft Univ. Press, 1993.

[15] Y. P. Raizer, *Gas Discharge Physics*. Berlin, Germany: Springer-Verlag, 1997.

[16] S. T. Zalesak, "Fully multidimensional flux corrected transport algorithms for fluids," *J. Comput. Phys.*, vol. 31, pp. 335–363, 1979.

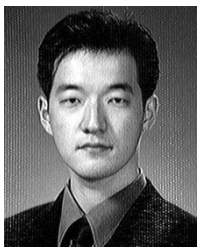

Woo Seok Kang was born in Seoul, Korea, in 1977. He received the B.S. and the M.S. degrees in nuclear engineering from Seoul National University, Seoul, in 2000 and 2002, respectively.

In 2002, he joined the Nuclear Technology Program in the Korea Institute of Science and Technology Evaluation and Planning (KISTEP), Seoul, where his current research interests include the planning and management of national R&D programs.

Jin Myung Park was born in Seoul, Korea, in 1972. He received the B.S. and M.S. degrees in nuclear engineering from Seoul National University, Seoul, in 1996 and 1998, respectively. He is currently working toward the Ph.D. degree in the Department of Nuclear Engineering, Seoul National University.

His research interests include the transport simulations of tokamak plasmas in nuclear fusion.

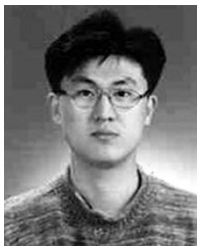

Yongho Kim was born in Yeasan, Korea, in 1970. He received the B.S., M.S., and Ph.D. degrees in nuclear engineering from Seoul National University, Seoul, Korea, in 1994, 1996, and 2002, respectively.

He is currently a Postdoctoral Researcher with the Korea Institute of Machinery and Materials, Daejeon, Korea. His research interests include the streamer dynamics generated by pulsed corona and dielectric barrier discharges.

Sang Hee Hong (M'88) received the B.S. degree in applied physics from Seoul National University, Seoul, Korea, in 1974, and the M.S. and Ph.D. degrees in electrical engineering from Colorado State University, Fort Collins, in 1975 and 1978, respectively.

In September 1979, he joined the College of Engineering, Seoul National University, where he is currently a Professor of nuclear engineering. He spent a year at the University of Sydney, Sydney, Australia, in 1989, as a Visiting Professor. His principal areas of research in the U.S. and Australia were stability analysis of MHD flows and theory of rotating plasmas and plasma centrifuges. His research interests in Korea moved to numerical modeling of tokamak plasmas and industrial processing plasmas. Recently, his research interests have included tokamak transport modeling and development of thermal and nonequilibrium plasma sources, as well as their material and environmental processing.